THE ASTROPHYSICAL JOURNAL, 430:13–28, 1994 July 20

BIAS PROPERTIES OF EXTRAGALACTIC DISTANCE INDICATORS. II. BIAS CORRECTIONS TO TULLY-FISHER DISTANCES FOR FIELD GALAXIES

ALLAN SANDAGE
The Observatories of the Carnegie Institution of Washington, 813 Santa Barbara Street, Pasadena, CA 91101
Received 1993 August 31; accepted 1994 January 21

ABSTRACT

Observational selection bias in samples of field galaxies used with the Tully-Fisher (TF) method of distance determination can be detected using the internal properties of the sample. The method is to divide the data into bins by line width and show that the apparent Hubble constant is multivalued *for different line widths* at given redshifts. The method is the same as used previously (Sandage 1988a, 1994) in samples composed of a fixed galaxy type by adding a fainter similar sample. If bias is present, the bias properties will disappear at a bright level but will reappear with the same properties at the corresponding fainter level. The procedure is generalized here to develop a method to determine statistically correct distances using the Tully-Fisher method.

A triple-entry correction to ridge-line TF absolute magnitudes is derived that depends on (1) redshift, (2) the apparent magnitude limit of the flux-limited sample, and (3) the line width. The Hubble constant will incorrectly be derived to increase outward and will also have too high a mean value if the intrinsic dispersion of the TF relation is either not accounted for at every redshift and every line width, or is underestimated.

The highest weight sample of field galaxies from the distance-limited 500 km s^{-1} catalog of Kraan-Korteweg & Tammann (1979) is used with the absolute calibration of the Tully-Fisher relation by Richter & Huchtmeier (1984) based on 64 galaxies in nearby groups, generally calibrated with Cepheids, to give a bias-free Hubble constant of $H_0 = 48 \pm 5$ km s^{-1} Mpc^{-1}. All other TF data for the *biased* samples of field galaxies discussed here show that the short distance scale with $H_0 \sim 85$ is not supported by the present TF calibration using the adopted intrinsic dispersion of the TF relation.

Unless the effects of observational bias in flux-limited samples are identified and corrected in each particular data sample, conclusions concerning both the Hubble constant and the existence of streaming motions about the cosmological expansion are suspect.

Subject headings: cosmology: observations — distance scale — galaxies: distances and redshifts — methods: statistical

1. INTRODUCTION

Most individual photometric distances for galaxies that are calculated using a fixed mean absolute magnitude, M_0, will be in error. The true absolute magnitude of any particular galaxy is not generally M_0 but is either brighter or fainter, spread in a distribution that is the luminosity function. Because of this, those galaxies that are intrinsically brighter than M_0 will have too small a calculated photometric distance. Intrinsically fainter galaxies will have too large a calculated distance. However, if the sample is truly distance-limited, and if M_0 is the proper mean absolute magnitude for such a sample, then the errors will be *symmetrically distributed about the correct value of log distance.* On the other hand, if the sample is from a flux-limited catalog, the distance errors, based again on M_0, will be distributed asymmetrically about a correct log of the mean distance because a part of the sample needed to obtain proper statistics will be missing from the catalog. This asymmetry, and therefore the error, will become larger with larger true distance, *progressively distorting the distance scale.*

The resulting bias is never absent in flux-limited samples. If it is not separately corrected *at each redshift*, the log Hubble constant calculated from the data will have too large a mean value, and will also appear to increase outward (de Vaucouleurs & Peters 1986; Giraud 1985, 1986a, b, c; Tully 1988) as an artifact (Teerikorpi 1984, 1987, 1990; Bottinelli et al. 1986) of an incorrect analysis.

Details of the problem and the method to correct it are the subject of the preceding paper (Sandage 1994, hereafter Paper I). It was shown there that the way to avoid the bias is to use a mean absolute magnitude, $M(m, v_i)$, that is a function of redshift for galaxies in a catalog whose limiting magnitude is m. The required correction is not the classical $M_0 - M(m)$ correction calculated by Malmquist (1920). If only a fixed absolute magnitude, $M(m)$ (even if "Malmquist-corrected"), is used at all redshifts rather than a correction that *depends on redshift*, the data will still give a calculated Hubble constant that incorrectly increases outward.

The required $M(m, v_i)$ absolute magnitudes needed to avoid bias can be found by considering the properties of the Spaenhauer diagram (SD). This diagram (Paper I, Figs. 2, 3, 4, and 11) is made by plotting the true absolute magnitudes (assumed here to be correctly calculated from redshifts; see § 2.2) against redshift for each entry in the catalog. It was shown in Paper I that the mean absolute magnitude, $M(m)$, calculated by Malmquist (1920) for a complete flux-limited sample is the average of the individual $M(m, v_i)$ absolute magnitudes over all redshifts, weighted by the relevant volume elements, the required individual $M(m, v_i)$ values thereby being lost.

The case discussed in Paper I was for a sample of objects of a given kind where M_0 is well defined, and where the dispersion $\sigma(M)$ in absolute magnitudes is small. Such a sample might be galaxies of a given morphological type and luminosity class.

The much more complicated case considered here is that in which individual distances are needed for galaxies in a sample

1994ApJ...430...13S

made up of a *mixture of types* in which M_0 varies within the mixture. In the case of the Tully-Fisher method of distance determination, the parameter introduced to narrow the luminosity function is the galaxian rotational velocity, often measured by the 21 cm line width (LW). When the data are divided into bins of LW, the division can be considered as equivalent to dividing the sample into separate galaxy "groups," each with its own proper M_0(LW) mean absolute magnitude.

The methods developed in Paper I can be applied *within each LW interval.* The bias properties of the complete Tully-Fisher sample can then be considered as a superposition of the bias properties of each individual Spaenhauer diagram as derived by the method in Paper I. The procedure for doing this is the subject of this paper.

A model for this much more complex bias correction is developed in the next section. The model is applied in § 3 to the 308 galaxy sample of Aaronson et al. (1982b). The bias corrections valid for it are derived from the internal properties of that sample.

The effect on the Hubble constant of either applying the corrections or neglecting them is discussed in § 4. Comparison of relative distance scales, with and without the corrections, are set out in § 5. The absolute value of the Hubble constant, based on two different catalogs, one flux-limited and the other distance-limited, is discussed in the penultimate section. An evaluation of the Tully-Fisher method to determine relative distances, and therefore the value of H_0 and the existence of putative streaming motions, is in the final section.

2. MODEL FOR THE BIAS CORRECTION AT EACH LINE WIDTH AND REDSHIFT

2.1. *Separate Spaenhauer Diagrams for Each Line Width*

Figure 1 is the Tully-Fisher (TF) diagram for the 308 galaxy sample of Aaronson et al. (1982b), shown as Figure 3 of Sandage (1988b, hereafter S88b). The absolute magnitudes are on the B_T photometric system, calculated using individual relative distances from the redshifts, corrected for Virgo "infall" and based on the arbitrary value of $H_0 = 50$ km s^{-1} Mpc^{-1}. The log line widths, defined at the 20% level of the 21 cm profile and reduced the edge-on orientation, are plotted as the abscissa.

The slope of the TF correlation for the subsample of 249 galaxies with log LW between 2.35 and 2.75 is $dM_B/d \log \mathrm{LW} = -6.77$ (S88b). The dispersion in M about the ridge line is $\sigma = 0.64$ mag. We now argue, as we did in S88b and will argue in the following paper (Federspiel, Sandage, & Tammann 1994, hereafter Paper III, § 8.4) that the true dispersion is at least this large, and that the scatter in Figure 1 is real, not an artifact of peculiar motions that would cause artificial scatter in the ordinate as has often been suggested.

2.2. *On the Value of* $\sigma(M)$ *in Figure* 1

The high value of the intrinsic dispersion is the central issue in the current debate on the distance scale. The larger this dispersion, the more severe are the selection bias errors in the distance scale.

Critics of the high value of $\sigma(M)$ at a given LW invoke noncosmological velocities (random and streaming) that would, if real, cause errors in the ordinate in Figure 1 whose size is $\Delta M = 2.17\, \Delta v / v_c$, where Δv is a putative noncosmological addition to v_c. It is said that such errors artificially increase the observed dispersion in M much above the value of the intrinsic dispersion. We argue against this point as follows.

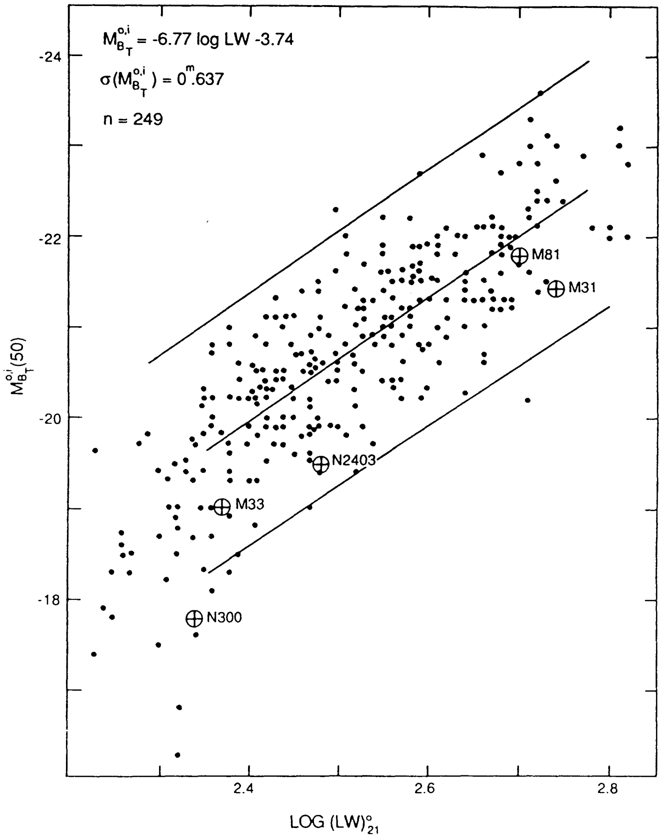

FIG. 1.—Correlation of absolute *B* magnitude (calculated from the redshift using $H_0 = 50$ km s^{-1} Mpc^{-1}) with line width, reduced to edge-on orientation for the 308 galaxy sample of Aaronson et al. (1982b). The five local calibrators are shown as circled crosses. They lie below the ridge line of the total sample due to observational selection bias for the reasons shown in Figs. 2 and 11*a*. The diagram is from Fig. 3 of S88b.

We contend that no streaming velocities on top of the cosmological flow have been detected except (1) the Virgo "infall" (see Tammann & Sandage 1985 for a review) and (2) the cosmic microwave background (CMB) dipole. Concerning the first, the redshifts of all galaxies in Figure 1 have been corrected for Virgo infall. Therefore, the absolute magnitudes in that diagram are on the corrected velocity system where the effects of the Virgo perturbation have been removed, certainly to first order, leaving only the errors due to *random* velocities. Note that the second effect within the relevant volume of $v < 2500$ km s^{-1} covered by the galaxies in Figure 1 does not enter the problem; the CMB dipole motion toward the hot CMB pole acts simply as an *offset*, since most of the region is, to first approximation, moving as a unit toward the hot CMB pole. No large *streaming* Δv velocities due to the CMB dipole exist for the Figure 1 galaxies, the "shear" component being small over this "local" region. (An extended discussion of this point is given in Paper III.) What then is the size of the *random* motions in the volume encompassed in Figure 1?

Random motions of galaxies in the very *local* field (i.e., $v_c < 500$ km s^{-1}) are inconsequentially small (Sandage 1986, 1987), giving $\sigma(\mathrm{random}) < 50$ km s^{-1}. Farther out in the extended region to $v \sim 2500$ km s^{-1}, the dispersion in the random velocities is smaller than can presently be measured because all extant determinations depend on the differences between the kinematic and the TF distances. Most of these differences must be interpreted not as real velocity perturbations but rather as errors in the photometric TF distances caused by the intrinsic dispersion in M(LW) of the TF relation, leading to systematic bias errors that increase with redshift—the subject of this and the following paper.

A limit can be put on the true random velocity component of the observed scatter by studying the characteristics of that scatter. If random motions were to dominate the dispersion in Figure 1, the distribution of the absolute magnitude residuals, M(kinematic) $-$ M(TF), would be wedge-shaped in the sense of closing toward high redshifts (see § 8.4 of Paper III), which is opposite to what is observed (see Figs. 9, 10, 12, 14, and 15 below).

Given this fact, we can put an upper limit to the effect of random motions on the determination of $\sigma(M)$ using kinematic distances. The error in M caused by a noncosmological velocity component, Δv, is $\Delta M = 2.17\,\Delta v/v$(cosmic). Even for an excessively high velocity *dispersion* of $\sigma(v_{\rm random}) = 200$ km s^{-1} (a gross overestimate for the *dispersion*, not the *range*, of the scatter), the ratio of Δv(random)/v(cosmic) is only 0.12, using the mean value of $\langle v(\text{cosmic})\rangle = 1600$ km s^{-1} for the Aaronson et al. (1982b) sample. Hence, the component of $\sigma(M)$ due to this random kinematic noise would be only $\sigma(M) = 0.3$ mag. Combining this artificially high $\sigma(M)$ due to random velocity errors, in the usual way as the square, with the data of Figure 1 shows that the observed dispersion of $\sigma(M) = 0.64$ can *at most* be too high by 12%. Furthermore, the more powerful evidence in Paper III is explicit that the true dispersion in the TF relation is as high as 0.9 mag for small LW, decreasing only to $\sim$0.4 mag for the highest line widths, which are very rare. An independent high-weight determination that $\sigma(M) \sim 0.7$ mag for the TF relation is also obtained from the data in local groups, calibrated via Cepheids (see § 6 below).

Why, then, do we differ with the conclusion of, say, Pierce & Tully (1992) that the true dispersion in the TF correlation is as small as $\sigma(M) = 0.3$ mag? The samples of galaxies in groups and clusters used by them are incomplete, reaching only a portion of the luminosity function of each aggregate, i.e., *all* galaxies at the fixed distance of each aggregate are not in their samples. The key point is that one must not confuse the two concepts of (1) a distance-limited sample and (2) an incomplete sample of galaxies at the same distance. Such incomplete samples, despite the common distance of the aggregate members, also suffer selection bias. The $\sigma(M)$ values derived from such samples are lower limits to the intrinsic dispersion.

2.3. *Consequences of an Intrinsic Dispersion for the TF Relation*

Figure 2 shows Figure 1 schematically (the zero points of the ordinate and abscissa are copied only approximately). Its purpose is to indicate how we can analyze each interval of LW as a separate bias problem by the method of Paper I, which treated only a *fixed* galaxy type.

Consider two intervals of line width, marked with hatching and labeled (1) and (2) in Figure 2. If the selection criterion for the total sample is by apparent magnitude (i.e., being flux-limited), then the galaxies *in each arbitrary LW interval will also be flux-limited.* The bias properties of a subsample within a given LW interval can, therefore, be found by plotting its own Spaenhauer diagram, as in Paper I, and as shown by the two inset diagrams in Figure 2. The *apex* magnitudes, shown by arrows, differ, being brighter for strip (2) than for strip (1). This is simply the ridge-line correlation of LW with absolute magnitude.

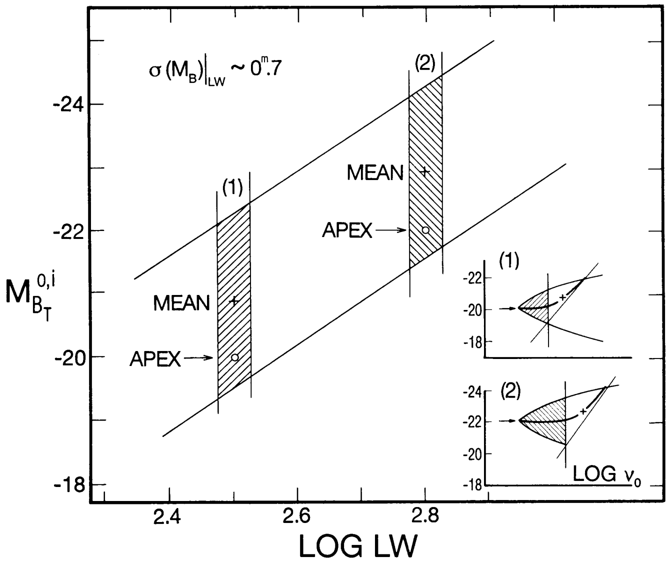

FIG. 2.—*Schematic* representation of Fig. 1, with the upper and lower envelope lines drawn and with two line-width intervals marked. The ordinate and abscissa zero points are not precisely the same as in Fig. 1. The apex magnitude (*arrow*) and the mean absolute magnitude (*plus sign*) of the entire sample are indicated in the Spaenhauer diagrams (absolute magnitude vs. redshift) in each inset.

Also shown within the insets are the mean absolute magnitudes, $M(m, \text{LW})$, for the separate samples within each LW interval. These are marked as plus signs in the nonhatched flux-limited part of the SD configurations. These, of course, are the separate Malmquist *mean* magnitudes given by the usual classical Malmquist calculation for $M_0 - M(m)$, but now required separately for each LW.

These mean magnitudes, $M(m, \text{LW})$, are also marked in the centers of strips (1) and (2) in Figure 2. The *apex* magnitudes, M_0(LW), marked as open circles in each strip, are, of course, fainter than the mean magnitudes, as shown also in the inset figures. The difference is the Malmquist $M_0 - M(m, \text{LW})$ correction itself.

Figure 2 shows why the positions of the ridge-line correlation of absolute magnitude versus LW (i.e., the TF relation itself) *differ as a function of redshift.* At low redshifts, the sample is distance-limited, outlined by the hatched areas of the inset diagrams in Figure 2. For these redshifts, the ridge lines pass through the marked *apex* positions (Fig. 2, *circles*). At higher redshifts *nonhatched areas*), the appropriate mean absolute magnitudes, $M(m, v_i, \text{LW})$, at any particular LW, move progressively brighter with redshift, first approaching the position of the "Malmquist mean" magnitude (*plus signs*) at the redshift of the crosses in the Figure 2 inset and then becoming even brighter at higher redshifts. (To visualize the effect and the method of constructing Figure 4 below, imagine binning the data by redshift and constructing separate TF relations for each bin.)

The fundamental fact that the appropriate absolute magnitudes become brighter at higher redshifts, *crucial to understanding the bias properties of TF samples*, was discovered observationally by Kraan-Korteweg, Cameron, & Tammann (1986, 1988). This central clue to the bias properties of *all TF samples that are flux-limited* is also seen in the Aaronson et al.

1994ApJ...430...13S

(1982b) sample later in this paper (§ 3), and was studied earlier (S88b), where the effect was demonstrated by dividing Figure 1 into two redshift regimes, separated at 500 km s^{-1} (S88b, Fig. 9).

This progressive brightening of the TF ridge lines as redshift increases is the needed bias correction, now at all line widths *and at each redshift*. The remainder of the paper is concerned with developing a model by which to make these triple-entry (magnitude, line width, redshift) corrections.

The procedure is to add individual Spaenhauer diagrams as defined in Paper I, one at a time, each valid for a particular LW interval, to form a grand SD with all LWs combined. To visualize the process, consider a "granular" start of this construction using the three LW intervals in Figure 3. This is a Spaenhauer diagram in which individual SD configurations, with upper and lower curved envelope lines drawn, are placed for the LW intervals centered on log LW values of 2.2, 2.5, and 2.8. A straight lower limit line at apparent magnitude $B = 14$ is common to the three individual SD configurations, cutting each configuration as shown. The volume-limited part of each configuration is the hatched area.

Figure 3 is schematic, although it is approximately correct in the vertical placement of the three apex magnitudes for the three configurations, i.e., the slope of the inferred Tully-Fisher relation defined by each of the apex positions is 4 mag for a line-width interval of 0.6 dex in Figure 1. This is $dM/d \log \mathrm{LW} = 6.67$, close to the observed slope in Figure 1 (S88b).

The horizontal position (i.e., the separation in redshift) of the three apices is arbitrary in Figure 3. In practice, the redshift separations are determined by the luminosity function of the galaxies in the sample, giving the ratio of the number of galaxies at log LW = 2.8 to those at 2.5 and 2.2. These ratios determine how much larger a volume (i.e., to what redshift) must be surveyed to include one galaxy (i.e., at the apex) at the particular LW for the particular SD to be plotted. But we show later (Figs. 6 and 7; see explanation in §§ 2.5 and 2.6) that the determination of the proper mean absolute magnitudes, $M(m, v_i, \mathrm{LW})$, needed to correct for selection bias is nearly independent of the horizontal placements of the separate Spaenhauer configurations.

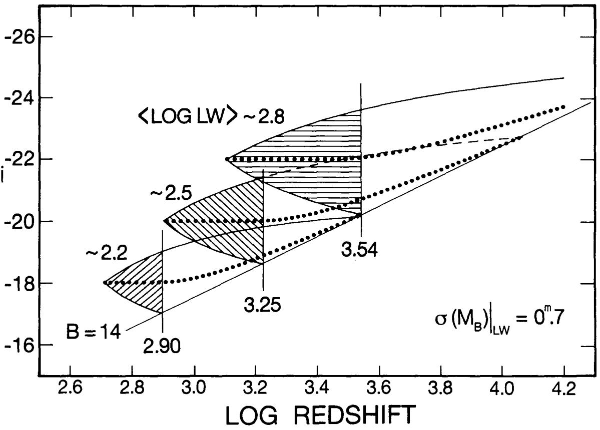

FIG. 3.—Schematic representation of the absolute magnitude distributions for three LW intervals as a function of redshift. Envelope lines are calculated for the three Spaenhauer configurations shown using $\sigma(M) = 0.7$ and the template curves in Paper I (Fig. 3 there). The vertical separation of the three apex positions is approximately 6.6 mag per dex of LW, which is close to the slope of the TF relation in Fig. 1. The hatched areas define the distance-limited subset of the total sample. The mean absolute magnitudes for any redshift are defined by the curves traced by dots in each of the three configurations.

The opening angle of each SD configuration is determined by the dispersion $\sigma(M, \mathrm{LW})$ of the TF relation at each LW (see Fig. 3 of Paper I). For the demonstration here we adopt a fixed dispersion of 0.7 mag for all LWs, similar to the value determined from the data themselves in the Aaronson et al. (1982b) sample (S88b) and in Paper III for the large Mathewson, Ford, & Buchhorn (1992) galaxy sample.

It is seen from Figure 3 that the bias-free subsamples at each LW (i.e., the hatched areas) *occur at different redshifts for different line widths*, marked and labeled by the log v values at the vertical lines which terminate each hatched area. This increase of the redshift of the distance-limited subsample as the LW increases means that the corrections for selection bias, determined by the methods of Paper I, are not only a function of redshift *but also a function of LW*. Such triple-entry corrections (i.e., they are also a function of the limiting apparent magnitude of the sample) have not generally been applied to any TF samples in discussions of the Hubble constant to date and in conclusions about putative streaming motions, claimed in the literature as deviations from a smooth cosmological expansion. It remains to be seen what effect these more detailed bias corrections will have on such conclusions in particular cases. However, we show in Paper III that applying the corrections to the large sample of Mathewson et al. (1992) eliminates the "backflow" of the putative Great Attractor by Dressler & Faber (1990a, b) and also gives a different interpretation to the 500 km s^{-1} cosmological offset obtained by Mathewson et al. (1992).

2.4. *The Two-Parameter Family of Corrections*

The individual proper $M(v_i, \mathrm{LW})$ absolute magnitudes are shown in Figure 3 as filled circles running with redshift in each of the three Spaenhauer configurations. The method of calculation of these loci is the same as that developed in Paper I (Table 1 and Figs. 4 and 5).

The $M(v_i, \mathrm{LW})$ loci within each of the *hatched areas* are straight lines placed at the level of the apex magnitudes. All data in the hatched areas are distance-limited. Larger redshifts define distances where the sample is progressively more flux-limited. The deeper cuts into each nonhatched area by the flux limit line at $B = 14$ show why the *proper* $M(v_i, \mathrm{LW})$ *absolute magnitudes become brighter as* v_i *increases.*

The family of proper absolute magnitudes, $M(m, v_i, \mathrm{LW})$, in Figure 4 is generated by reading each of the three curves in Figure 3 at different redshifts, and interpolating between the three discrete line-width configurations, giving a continuous abscissa as the independent variable. The log redshift values are marked inside the vertical border to the left of each curve. The model in Figure 4 is based on the level of B_{limit} assumed in Figure 3. Hence, these schematic *model* corrections are good only for such an ideal catalog that is complete to a given apparent magnitude ($B = 14$ here), and whose data conform to Figure 2, which itself is schematic. From this it is clear why these corrections themselves are functions of the limiting catalog magnitude, labeled B_{limit} here. We treat a real case using actual data later in Figures 9–13. The purpose in this section is only to explore the predictive properties of the schematic model.

Figure 4 is a Tully-Fisher diagram showing the ridge-line correlations of the data *binned by redshift*. The ordinate is the

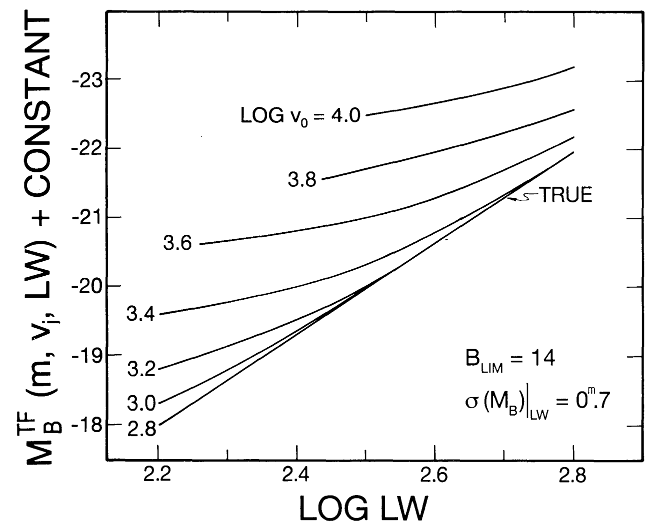

FIG. 4.—Predicted Tully-Fisher correlation as a function of redshift based on the schematic model in Figs. 2 and 3. The mean log redshift values at the center of each redshift interval into which the data were binned are marked at the left of each curve. The curves are generated by reading Fig. 3. The straight line marked "true" is the mean Tully-Fisher correlation (the ridge line) valid for the *volume-limited* subsample defined by the hatched areas in Fig. 3. The magnitudes along this line are the "apex" magnitudes, M_0(LW). This only applies to the distance-limited subset of any total sample. The complete family of curves defines the corrections needed at every line width and every redshift to avoid errors in photometric distances due to selection bias of non–distance-limited subsets of a total sample.

proper mean absolute magnitude that is valid for a subsample that has the mean redshift labeled for each curve, for various line widths (*abscissa*). The line labeled "true" is the ridge-line TF correlation for the distance-limited part of the sample[1] (i.e., within the hatched areas of Fig. 3). The proper mean absolute magnitudes to be used for all other galaxies in the sample, $M(m, v_i, \mathrm{LW})$, are given by the other curves of the family.

Figure 4 contains the principal result we seek. It shows many of the important aspects of the bias properties of TF samples. For example, it explains the central effect, mentioned earlier and discovered empirically by Kraan-Korteweg et al. (1986, 1988), that the ridge-line absolute magnitudes in the TF correlation of the sample they analyzed *moves brighter for increasing redshift*. It also explains the result (S88b, Fig. 9) that *the lowest redshift galaxies lie at the faintest absolute magnitudes at a given LW in the TF relation.*

The calibration of the TF ridge line using local galaxies such as M31 and M33 (Sandage & Tammann 1976; Freedman 1990) *refers only to this lowest redshift subsample* (i.e., the calibrating sample is distance-limited) of the complete TF sample. As said before, failure to correct the high-redshift galaxies for the offset due to bias, *now at every redshift and at each LW*, will give too large a mean Hubble constant and a fake signal that the Hubble constant increases outward.

Figure 4 is plotted in a different representation in Figure 5, where the abscissa is redshift and the generator of the curves is log LW. Figure 5 is an easier diagram from which to read, by interpolation, the needed bias-free absolute magnitudes. Figure 5 is the double-entry (redshift, LW) equivalent of Table 1 of Paper I for this specific schematic model with $B_{\mathrm{limit}} = 14$ and $\sigma(M_0) = 0.7$ mag.

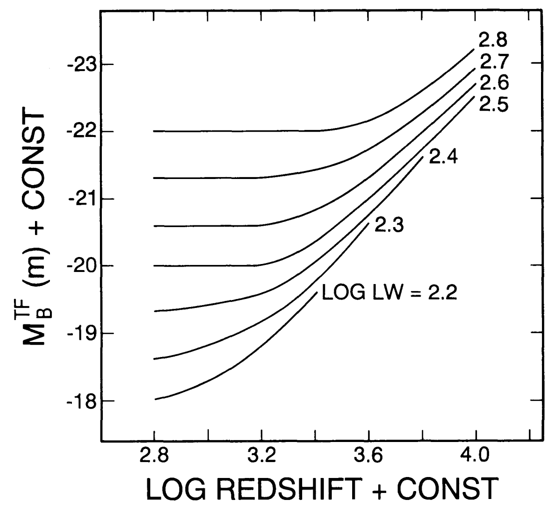

FIG. 5.—Same as Fig. 4, but in the different representation of the series of Spaenhauer diagrams for different line widths. The diagram shows the predictions from the schematic model of Figs. 2 and 3. The diagram using real data is Fig. 13.

2.5. *The Insensitivity of the Corrections to the Placement of the Spaenhauer Configurations in Figure 3*

As mentioned earlier, the horizontal placement of the apex positions of the individual Spaenhauer configurations in Figure 3 is determined by the ratios of the number of galaxies in a volume-limited sample in each of the LW intervals. This is given by the luminosity function because the line widths are related, to within the scatter, to absolute magnitudes by the Tully-Fisher ridge-line correlation itself. We now explore the sensitivity of the correction curves in Figures 4 and 5 to the horizontal placement of the apices in Figure 3.

An extreme example of the placement is shown in Figure 6, where the redshifts of the apices are assumed to be the same at log $v = 2.7$ for the three LW intervals. The ridge lines (the mean TF relation) at every redshift, read from Figure 6, are

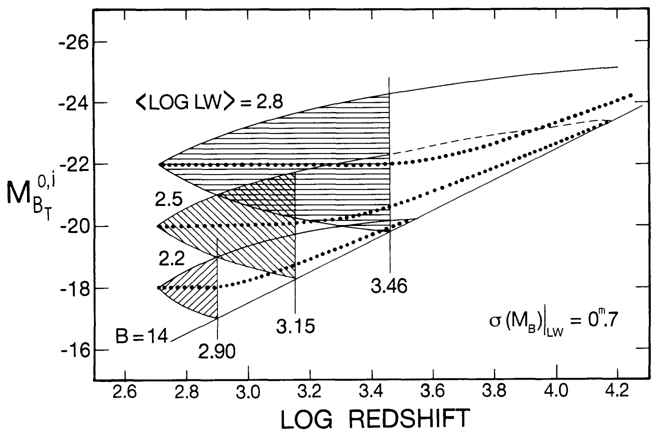

FIG. 6.—Same as Fig. 3 in principle, but with a different assumption for the horizontal placement of the three schematic Spaenhauer configurations for the three marked line widths.

---

[1] The distance-limited regime of any catalog can always be identified in any sample by drawing individual Spaenhauer diagrams for each line width and constructing the envelope lines and the flux limit line to find their intersections empirically, defining the hatched area. All galaxies within that area define a bias-free, distance-limited subsample of any particular catalog. The method is used later in Figs. 9 and 10 (see § 3) and extensively in Paper III.

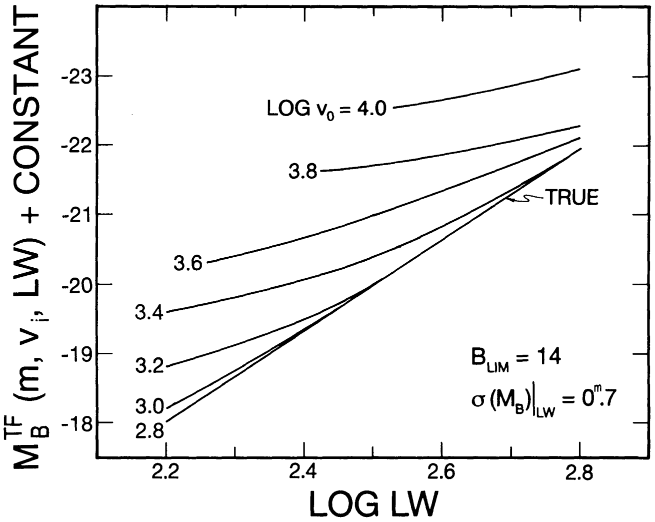

FIG. 7.—Same as Fig. 4, showing the required absolute magnitudes needed to avoid errors in photometric distances due to selection bias, but for the configurations set out in Fig. 6, based on the model in Figs. 2 and 6. Figs. 4 and 7 are nearly the same, for the reason discussed in the text.

shown in Figure 7 in the same way that Figure 4 was derived from Figure 3.

As in Figure 3, the hatched areas in Figure 6 show the volume-limited subset of the total sample for each LW interval. The redshifts at this transition are nearly the same in Figure 3 and in Figure 6 at the same respective LW intervals, shown by the markings of the transition redshifts in the two diagrams.

Nevertheless, the fraction of the total sample at a given LW that is volume-limited is larger in Figure 6 than in Figure 3 because of the relation of the positions of the lower envelopes to the flux limit line at $B = 14$. Study of the geometries of each diagram shows why this is so.

The consequence is that the mean absolute magnitudes at each redshift for each interval of LW, shown by the loci marked by the black dots, are very nearly the same in both Figures 3 and 6. Hence, the corrections in Figure 5 are nearly independent of the horizontal placement of the individual Spaenhauer configurations in Figures 3 and 6, and therefore are nearly independent of the luminosity function. Said differently, the correction curves in Figure 5 also nearly satisfy the data in Figures 6 and 7, showing why Figures 4 and 7 are nearly identical.

2.6. *The Apparent Hubble Constant as a Function of Redshift and LW if the Bias Corrections Are Ignored*

The curves in Figures 4 and 7 are summarized in Table 1, which lists the proper absolute magnitude $M(v_i, \mathrm{LW})$ that must be used to avoid bias at every redshift and at every LW. These absolute magnitudes are determined for this specific schematic model whose $M_0(\mathrm{LW})$ absolute magnitude zero points [and $\sigma(M)$ values] are shown in Figures 3 and 6.

Table 1 is constructed by reading Figure 4, based on Figure 3. It is important to note that the equivalent of Figures 3 and 4 must be generated from *each* sample of real data, as illustrated in § 3 for the Aaronson et al. (1982b) sample.

The entries in Table 1A for the lowest three redshift intervals (log v = 2.8, 2.9, and 3.0) are the apex magnitudes, M_0(LW), of each individual Spaehauer diagram at the different LW values.

TABLE 1A

BIAS-FREE $M(v_i, \mathrm{LW})$ ABSOLUTE MAGNITUDES FOR THE MODEL IN FIGURES 3 AND 4

	log LW						
log v_i	2.2	2.3	2.4	2.5	2.6	2.7	2.8
2.8....	−18.00	−18.60	−19.30	−20.00	−20.60	−21.30	−22.00
3.0....	−18.26	−18.80	−19.40	−20.00	−20.60	−22.38	−22.00
3.2....	−18.80	−19.10	−19.55	−20.00	−20.60	−21.30	−22.00
3.4....	−19.60	−19.78	−20.00	−20.30	−20.80	−21.40	−22.00
3.6....	...	−20.65	−20.83	−21.00	−21.30	−21.70	−22.15
3.8....	...	...	−21.50	−21.72	−22.00	−22.25	−22.60
4.0....	...	...	...	−22.50	−22.68	−22.90	−23.20

TABLE 1B

CORRECTIONS NEEDED TO M_0(LW) TO AVOID SELECTION BIAS

	log LW			
log v_i	2.2	2.4	2.6	2.8
2.8..........	0.00	0.00	0.00	0.00
3.0..........	0.26	0.10	0.00	0.00
3.2..........	0.80	0.25	0.00	0.00
3.4..........	1.60	0.70	0.20	0.00
3.6..........	...	1.53	0.70	0.15
3.8..........	...	2.20	1.40	0.60
4.0..........	...	...	2.08	1.20

TABLE 1C

APPARENT HUBBLE CONSTANT IF BIAS CORRECTIONS ARE NOT APPLIED

	log LW			
log v_i	2.2	2.4	2.6	2.8
2.8..........	50	50	50	50
3.0..........	56	52	50	50
3.2..........	72	56	50	50
3.4..........	105	69	55	50
3.6..........	...	101	69	54
3.8..........	...	138	95	66
4.0..........	...	...	132	87

We emphasize again that these data refer only to the volume-limited subset of the complete sample.

The bias corrections that must be applied to the M_0(LW) magnitudes at larger redshifts are obtained from Table 1A by subtracting all other entries from the values in the top row, as listed in Table 1B. These are the magnitude differences in Figure 4 between the TF calibration for the volume-limited sample, marked "true" in Figure 4, and the ridge-line curves at each larger redshift and at every LW.

Systematic errors in a distance scale that result by failing to apply Table 1A will translate to errors in the derived Hubble ratios as $\Delta \log H = 0.2\,\Delta M$. Adopting a local value for H_0 of 50 km s^{-1} Mpc^{-1} gives the incorrectly derived (apparent) values of H listed in Table 1C and shown in Figure 8, if the bias corrections are ignored.

Note that for any redshift greater than log $v = 2.8$, the uncorrected Hubble constant will be multivalued, depending on both line width and redshift. This is the decisive signal that observational bias is present. Said differently, if bias is present, the apparent value of the calculated mean value of the Hubble

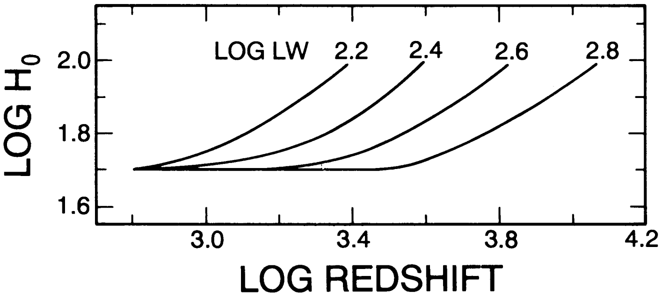

FIG. 8.—Apparent value of the log Hubble constant on the arbitrary scale of $H_0 = 50$ km s^{-1} Mpc^{-1} that would be derived using the indicated line-width intervals at each redshift if the bias corrections of Figs. 4 and 5 were not applied. Without bias corrections, the derived Hubble constant is multivalued at a given redshift, which is a contradiction. This is the signal that observational selection bias is present. The value $\log H_0 = 1.7$ corresponds to $H_0 = 50$ km s^{-1} Mpc^{-1}, assumed throughout this paper.

constant will differ systematically between subsets of the total data when *analyzed separately in different bins of LW*. We use this method to show the presence of selection bias in the large sample by Mathewson et al. (1992 in Paper III, Figs. 1 and 2).

3. APPLYING THE MODEL TO THE 308 GALAXY SAMPLE OF AARONSON ET AL.

3.1. *Explicit Method to Determine the Bias Properties of This Tully-Fisher Field Galaxy Sample*

We now analyze the data from the Aaronson et al. (1982b) catalog shown in Figure 1. The purpose is to illustrate the procedure and to show that the predictions of the model are (1) verified in detail, (2) powerful in identifying the bias, and (3) an exemplum in using the method for detecting the presence of bias in any sample using any nonkinematic method of distance determination.

The method for TF samples is to bin the catalog into LW intervals and redshift and to show that the Hubble constant is multivalued at each redshift and LW in the absence of bias corrections. The vehicle of demonstration is the Spaenhauer diagram. Both the *B*- and *H*-band photometric data are analyzed in this way.

Figure 9 shows four typical SDs where absolute magnitudes, calculated from redshift distances using $H_0 = 50$, are plotted against log redshift. The galaxies in these subsamples are of course, spirals and cover a large range of Hubble types along the spiral sequence. The absolute magnitudes are on the B_T system, and have been corrected for Galactic absorption and for internal self-absorption by the precepts of the RSA (Sandage & Tammann 1981, 1987). The needed apparent B_T magnitudes have been taken either from the RSA or from the Kraan-Korteweg (1986a, b) Catalog of 2810 Nearby Galaxies.

The redshifts, v_{220}, are the velocities relative to the Local Group but corrected to the Virgocentric frame by the precepts of the Kraan-Korteweg (KK) model using an infall velocity of 220 km s^{-1} (Tammann & Sandage 1985; Sandage & Tammann 1990). We assume a noiseless cosmological linear expansion in the Virgocentric frame, justified in general in Paper I, and in particular in Paper III (footnote 4) for the approximation needed here. (Note the relation of this procedure to the problem of the CMB dipole, discussed in § 2.2 above and in § 8 of Paper III.)

The upper and lower curved envelope lines in Figure 9 have been drawn by eye by the method of Paper I (Fig. 3). The vertical lines divided each configuration into the distance-limited and flux-limited regions in the usual way. The straight-line loci for the apparent magnitude cutoffs have been determined by a best fit to the data, again by inspection.

Arrows mark the estimated apex position for each of the four Spaenhauer configurations. These apex absolute magnitudes define bias-free Tully-Fisher ridge lines that are, of course, valid only for the distance-limited subsample of the data. They correspond to the lines marked "true" in Figures 4 and 7.

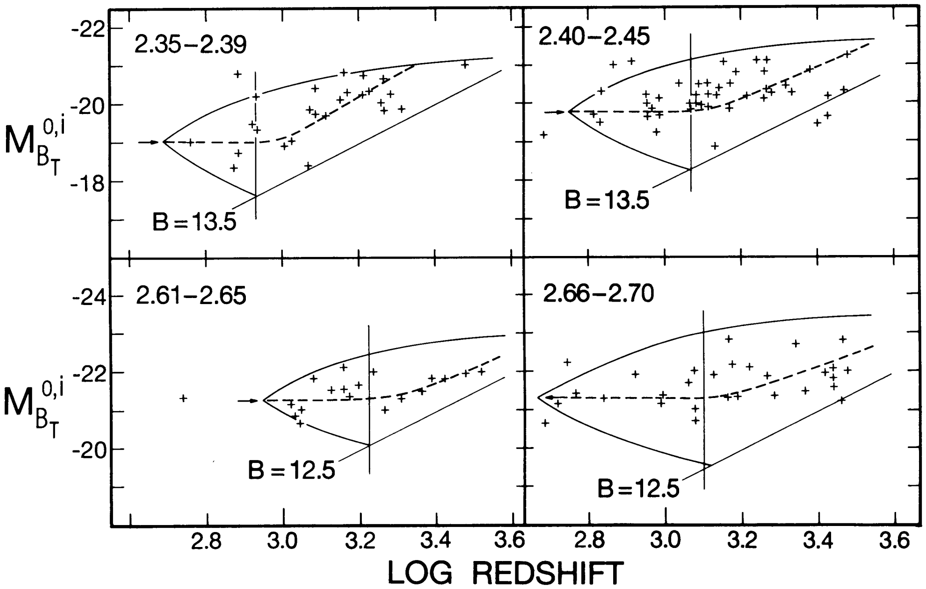

FIG. 9.—Distribution of calculated kinematic blue absolute magnitudes in the Aaronson et al. sample as a function of redshift and discrete intervals of log line width, marked at the upper left of each panel. The upper and lower envelope lines are calculated by the model of Paper I (Fig. 3 and Table 1). The lower straight apparent magnitude limit lines are drawn by eye to enclose the data. The vertical line in each panel separates the distance-limited region from the flux-limited region that is always present at larger redshifts. The dashed lines define the empirical mean absolute magnitudes needed to calculate bias-free photometric distances.

TABLE 2

Apex Absolute Magnitudes for Nine Bias Configurations Used in Figure 11

log LW	M_B^{50}(Apex)	M_H^{50}(Apex)
2.37................	−19.3	−20.6
2.425..............	−19.8	−21.0
2.48................	−19.9	−21.7
2.53................	−20.2	−22.3
2.58................	−20.8	−23.2
2.63................	−21.0	−23.4
2.68................	−21.4	−23.8
2.73................	−21.8:	−24.7
2.80................	−22.2:	−24.7

The mean absolute magnitudes, $M(v_i, \mathrm{LW})$, needed to obtain bias-free magnitudes at every redshift and every line width are shown in Figure 9 as thin dashed lines within the borders of the configurations. In a large enough data sample, these positions can be determined empirically by the distribution of the data themselves, i.e., they need not be calculated from the theoretical model of Paper I (Table 1 and Fig. 4 of that paper). However, in the present case there are too few points in the Aaronson et al. catalog within any given LW interval to rely entirely on the actual mean values at each redshift, as is done strictly in Paper III. Hence, the placement of parts of the curves in Figure 9, and in Figures 10 and 12 below, was partially guided by the expectations from Figure 4 of Paper I (Fig. 4).

The individual apex M_0(LW) magnitudes for each LW are determined directly from the Spaenhauer diagrams in § 3.2. These permitted the combining of the correction curves for all redshifts and all line widths into a double-entry correction table (Table 3; see § 3.3).

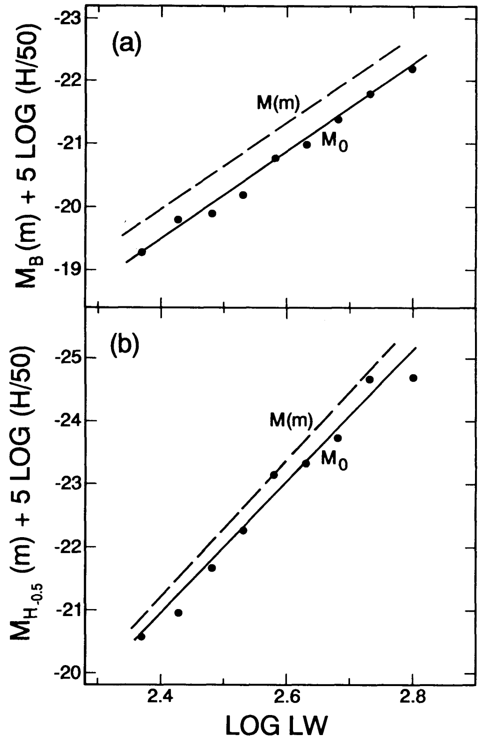

Fig. 11.—(*a*) Ridge lines of the mean Tully-Fisher correlation in the *B* photometric band from the data in Table 2. The distance scale used for the oridinate is relative, based on $H_0 = 50$. The least-squares line marked M_0 has the equation $M_{B_T}^{0,i}(H_0 = 50) = -6.86 \log \mathrm{LW} - 3.02$. The ridge line for the complete flux-limited sample, marked $M(m)$, has the equation $M_{B_T}^{0,i} = -6.77 \log \mathrm{LW} - 3.74$, which is eq. (1) of S88b. (*b*) Same for *H*-band apex magnitudes. The least-squares line marked M_0 has the equation $M_H(H_0 = 50) = -10.56 \log \mathrm{LW} + 4.37$. The line marked $M(m)$ is the mean for the entire (flux-limited) sample. Its equation is $M_H = -10.84 \log \mathrm{LW} + 4.82$, which is eq. (2) of S88b.

3.2. *The Bias-free Slope of the TF Correlation*

The estimated apex absolute $M_0(B)$ magnitudes for the nine LW intervals, of which four are shown in Figure 9, are listed in Table 2. Similar data for the *H* photometric band, determined in the same way and illustrated by the two examples in Figure 10, are also listed in that table. These ridge-line, bias-free absolute magnitudes are plotted in Figures 11*a* and 11*b*, and marked M_0, corresponding to the "true" lines in Figures 4 and 7.

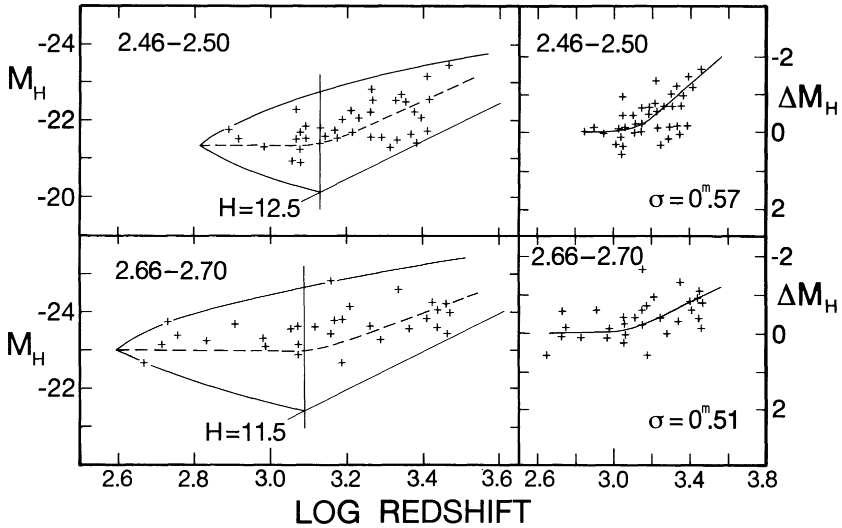

Fig. 10.—Same as Fig. 9, but for magnitudes in the *H* photometric band listed by Aaronson et al. (1982b). The panels at the right show the same data as those at the left but are plotted as magnitude differences from the apex absolute magnitude. These are the differences, *M*(kinematic) − *M*(TF), between absolute magnitudes computed from the redshifts and alternatively from the TF ridge line, i.e., using the M_0(LW) *apex* magnitudes (Fig. 11*b*). The dashed lines define the adopted mean absolute magnitude corrections at each redshift.

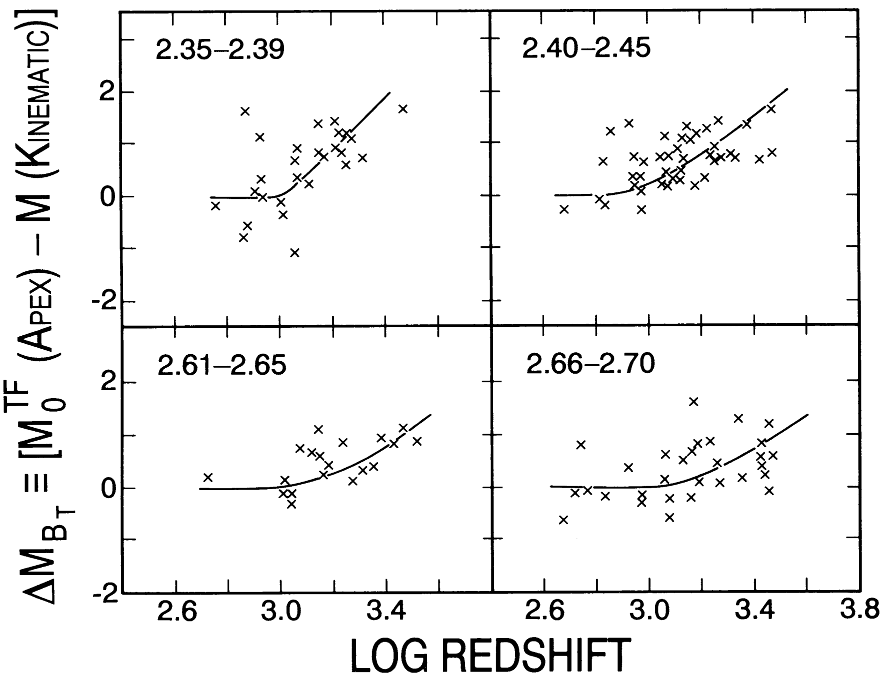

FIG. 12.—Mean corrections to M_0 for B-band magnitudes as a function of redshift for the marked LW intervals using data from the Aaronson et al. sample. These are the *real* equivalents of the *model* expectations of Figs. 4 and 5. The ordinate is the difference between magnitudes calculated from ridge-line TF distances and from redshift distances.

Also shown and marked as $M(m)$ in both panels of Figure 11 are the *mean* lines through the entire sample in B and H as calculated and discussed elsewhere (S88b). The equations of the lines are given in the legend to Figure 11 and in § 6 below.

The difference between M_0 and $M(m)$ in each of the panels would, of course, be the Malmquist (ensemble) correction if the Aaronson et al. sample had been properly selected to be strictly flux-limited. However, the sample is not so well defined statistically because subsamples were added for vatious reasons during the process of observation, as discussed by the authors of the catalog. Hence, the Malmquist (ideal) equation is not expected to apply *strictly* to the Aaronson et al. sample.

However, for any sample, no matter how selected, we can always determine the bias corrections by the empirical method set out in this paper, no appeal being needed to an analytical formulation which necessarily depends on precepts in the selection criteria. The present method via Spaenhauer diagrams is, then, nearly "self-revealing."

The difference between M_0 and $M(m)$ in Figure 11 varies between 0.2 and 0.4 mag. This is approximately the Malmquist idealized value of $M_0 - M(m) = 1.386\sigma(M)^2$ if $\sigma(M) = 0.5$ mag. But it is our contention that this dispersion, averaged over all line widths, is too small by about a factor of ~ 1.5 as determined earlier from the complete sample (S88b) and justified in § 2.2.

An explanation of why M_0 and $M(m)$ in Figures 11*a* and 11*b* are closer together than they would be in a strictly flux-limited sample in a space uniformly filled with galaxies and with galaxies whose true TFF dispersion is $\sigma(M) = 0.7$ mag is, it would seem, that the Aaronson et al. sample is not ideal in that way. There clearly are too few galaxies in Figures 9, 10, and 12 at high redshifts, showing the incompleteness of the sample at these redshifts. The consequence is that the measured $M(m, \mathrm{LW})$ mean magnitudes are *fainter* in Figure 11 than they would be for an ideal sample. If, in fact, $\sigma(\mathrm{true}) = 0.7$ mag, as derived for the large sample in Paper III, then the Malmquist difference $M(m) - M_0$ would be 0.68 mag.

3.3. *The Family of Correction Curves at Each Redshift and Line Width*

Figure 12 shows a sample of the individual correction curves to $M_0(\mathrm{LW})$ for the four LW intervals shown in Figure 9. The data in Figure 12 are the same as those plotted in Figure 9 but are zero-pointed for the distance-limited part of the sample, i.e., the curves are flat at small redshifts and are normalized to $M(\mathrm{TF}) - M(\mathrm{kinematic}) = 0$ at these redshifts.

An important property of the curves in Figure 12 is the progressive decrease in the slopes, $d\Delta M/d \log v$, of the high-redshift parts of the $M(\mathrm{TF}) - M(\mathrm{kinematic})$ curves as the LWs increase from log LW = 2.37 to log LW = 2.68. This behavior is predicted by the model from Figures 4, 5, and 7, seen by noting that at small LW (at left in the diagrams) the separations in the ordinate between the curves of constant redshift are larger than the separations read at larger LW.[2]

The data conform well with this central prediction of the model, and the result is equivalent to stating that the slope of the TF relation itself must depend on redshift, as is explicit in Figures 4 and 7.

---

[2] The concomitant effect is that the slope, dM/d log LW, of the TF relation itself for the total (flux-limited) sample will differ from the *bias-free* (correct) slope, marked "true" in Figs. 4 and 7. This problem of finding the bias-free slope from any sample has been discussed by Schechter (1980; see also Aaronson et al. 1982a), where he set out the method using the "inverse" TF relation, done by regressing LW on magnitude rather than magnitude on LW.

The conclusion by Tully (1988) that simply determining the correct (bias-free) *slope* removes the bias is not correct. The bias properties within the TF correlation remain (Figs. 4, 7, and 13) as a function of redshift. These are the corrections we derive here.

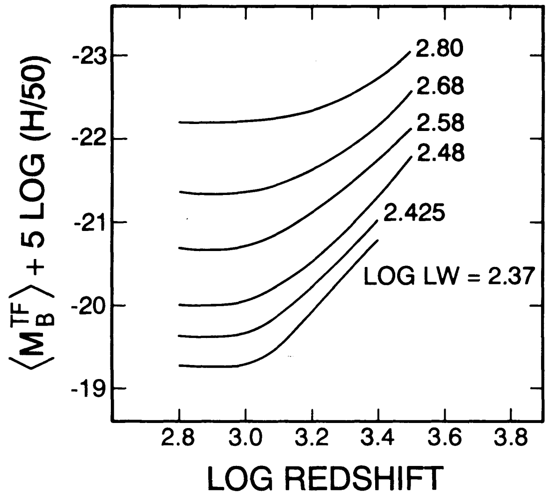

FIG. 13.—Summary of the empirical corrections to M_0(LW) for each LW interval at each redshift from data in the Aaronson et al. sample, determined by reading the mean curves in the H band similar to those in Fig. 9. The shapes of these curves derived from actual data agree with the model expectations in Fig. 5.

Figure 13 shows the result of combining the separate correction curves for the actual Aaronson et al. data, and using the apex M_0 magnitudes defined by the least-squares solution of Figure 11*a* (i.e., the Table 2 values) to set the zero points along the ordinate. The mean log LW values are marked at the right of each curve.

The similarity of the curves in Figure 13 determined from the data to those in Figure 5 from the *schematic model* is excellent, and is clearly a test of the model.

The corrections in B, read from Figure 13, are listed in Table 3. Similar correction curves in H, calculated in the same manner using all the Spaenhauer configurations in H (Fig. 10, for example) are given in Table 4.

4. EFFECTS OF THE CORRECTIONS ON THE HUBBLE CONSTANT

Failure to apply the Figure 13 corrections has the consequences for the Hubble constant discussed in Paper I (see Figs. 12 and 13 there). Figure 8 here shows the *model* expectations for the value of H_0 using the TF method. Figure 14 shows the *actual* B-band H_0 ratios calculated galaxy by galaxy from the Aaronson et al. sample for galaxies within the log LW interval from 2.35 to 2.39. The data are the same as those in the upper left-hand panel of Figure 9.

The upper panel in Figure 14 shows the apparent increase of $\langle H \rangle$ with increasing redshift beyond log $v = 3.0$. The lower panel with its guiding limit lines shows the effect of selection bias. Note that the lower panel in Figure 14 is a different representation of the Spaenhauer diagram of Figure 9.

The mean line through the data in Figure 14, beginning at the apex and remaining flat until log $v = 3.0$, is the mean absolute magnitude line in Figure 9, multiplied by 0.2 and arbitrarily zero-pointed to give $H_0 = 50$ (log $H_0 = 1.7$) at the apex. The selection bias due to the flux limitation at $B = 13.5$ is clear for redshifts larger than log $v_{220} = 3.0$.

TABLE 3

BIAS-FREE ABSOLUTE M_B MAGNITUDES TO BE USED WITH THE AARONSON ET AL. SAMPLE TO AVOID SYSTEMATIC ERRORS IN PHOTOMETRIC DISTANCES

	log LW								
log v_i	2.37	2.425	2.48	2.53	2.58	2.63	2.68	2.73	2.80
A. B-Band Absolute Magnitude Differences from M_0(LW)									
2.8	0.00	0.00	0.00	0.00	0.00	0.00	0.00	0.00	0.00
2.9	0.00	0.00	0.00	0.00	0.00	0.00	0.00	0.00	0.00
3.0	0.00	0.00	0.00	0.00	0.00	0.00	0.00	0.00	0.00
3.1	0.31	0.27	0.22	0.18	0.14	0.10	0.06	0.02	0.00
3.2	0.67	0.59	0.48	0.44	0.40	0.34	0.28	0.20	0.14
3.3	1.12	1.02	0.89	0.80	0.70	0.62	0.50	0.39	0.29
3.4	1.52	1.38	1.27	1.12	1.03	0.89	0.77	0.64	0.48
3.5	...	...	1.77	1.62	1.47	1.32	1.20	1.00	0.82
B. B-Band Absolute $M(v_i$, LW) Magnitudes									
Apex	−19.28	−19.66	−20.03	−20.38	−20.72	−21.06	−21.40	−21.75	−22.23
2.8	−19.28	−19.66	−20.03	−20.38	−20.72	−21.06	−21.40	−21.75	−22.23
2.9	−19.28	−19.66	−20.03	−20.38	−20.72	−21.06	−21.40	−21.75	−22.23
3.0	−19.28	−19.66	−20.03	−20.38	−20.72	−21.06	−21.40	−21.75	−22.23
3.1	−19.59	−19.93	−20.25	−20.56	−20.86	−21.16	−21.46	−21.77	−22.25
3.2	−19.95	−20.25	−20.51	−20.81	−21.12	−21.40	−21.68	−21.95	−22.37
3.3	−20.40	−20.68	−20.92	−21.18	−21.42	−21.68	−21.90	−22.14	−22.52
3.4	−20.80	−21.04	−21.30	−21.50	−21.75	−21.95	−22.17	−22.39	−22.71
3.5	...	...	−21.80	−22.00	−22.19	−22.38	−22.60	−22.75	−23.05
C. Apparent Hubble Constant if B-Band Bias Corrections Are Not Applied									
2.8	50	50	50	50	50	50	50	50	50
2.9	50	50	50	50	50	50	50	50	50
3.0	50	50	50	50	50	50	50	50	50
3.1	58	57	55	54	53	52	51	51	50
3.2	68	66	63	61	60	59	57	55	53
3.3	84	80	76	72	69	67	63	60	57
3.4	101	95	90	84	80	76	71	67	63
3.5	...	...	113	106	99	92	87	79	73

TABLE 4

BIAS-FREE ABSOLUTE M_H MAGNITUDES TO BE USED WITH THE AARONSON ET AL. SAMPLE TO AVOID SYSTEMATIC ERRORS IN PHOTOMETRIC DISTANCES

	log LW								
log v_i	2.37	2.425	2.48	2.53	2.58	2.63	2.68	2.73	2.80
A. *H*-Band Absolute Magnitude Differences from M_0(LW)									
2.8	0.00	0.00	0.00	0.00	0.00	0.00	0.00	0.00	...
2.9	0.00	0.00	0.00	0.00	0.00	0.00	0.00	0.00	...
3.0	0.00	0.00	0.00	0.00	0.00	0.00	0.00	0.00	...
3.1	0.12	0.11	0.08	0.07	0.06	0.05	0.02	0.00	...
3.2	0.36	0.27	0.24	0.22	0.17	0.12	0.11	0.04	0.00
3.3	0.73	0.64	0.53	0.48	0.41	0.32	0.27	0.21	0.12
3.4	1.11	1.04	0.93	0.83	0.70	0.58	0.47	0.38	0.20
3.5	...	...	1.50	1.25	1.13	0.90	0.77	0.55	0.30
B. *H*-Band Absolute $M(v_i$, LW) Magnitudes									
Apex	−20.66	−21.24	−21.82	−22.35	−22.87	−23.40	−23.93	−24.46	−25.20
2.8	−20.66	−21.24	−21.82	−22.35	−22.87	−23.40	−23.93	−24.46	−25.20
2.9	−20.66	−21.24	−21.82	−22.35	−22.87	−23.40	−23.93	−24.46	−25.20
3.0	−20.66	−21.24	−21.82	−22.35	−22.87	−23.40	−23.93	−24.46	−25.20
3.1	−20.78	−21.35	−21.90	−22.42	−22.93	−23.45	−23.95	−24.46	−25.20
3.2	−21.02	−21.51	−22.06	−22.57	−23.04	−23.52	−24.04	−24.50	−25.20
3.3	−21.39	−21.88	−22.35	−22.83	−23.28	−23.72	−24.20	−24.67	−25.32
3.4	−21.77	−22.28	−22.75	−23.18	−23.57	−23.98	−24.40	−24.84	−25.40
3.5	...	...	−23.32	−32.60	−24.00	−24.30	−24.70	−25.01	−25.50

Figure 15 shows the same effect of an apparent increase of H_0 outward, again for *B* magnitudes, but now for the larger line-width interval between log LW values of 2.66 and 2.70. The slope of the apparent increase log *H* with redshift is now much smaller than in Figure 14, *as predicted from the model* (explained in § 3.3) and shown above in Figure 8. As before, the reason is the *difference of slopes of the curves in Figures 4 and 7* between small and large LW at different redshifts.

The curves from the bottom panels of Figures 14 and 15, combined with other similar data and averaged, are shown in the composite summary in Figure 16 of how the calculated H_0 depends on redshift and LW for uncorrected data. The comparison with the *expectation* diagram from the model in Figure

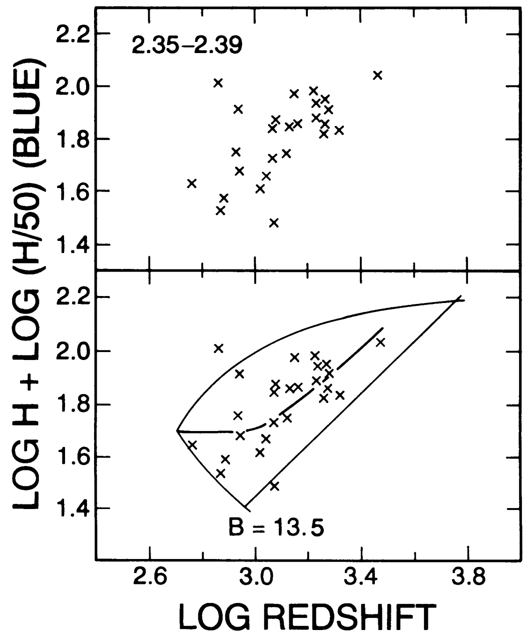

FIG. 14.—*Top*: Apparent variation of the log Hubble constant with increasing redshift for galaxies in the Aaronson et al. sample with line widths in the interval of log LW from 2.35 to 2.39, using only the M_0 apex absolute magnitude at all redshifts in the calculation of photometric distances. *Bottom*: Same data points as above, but with limit lines calculated in an obvious way from the upper left-hand panel of Fig. 9. The apparent increase of *H* outward is not real but is due to observational selection bias. Data that would be to the right of the $B = 13.5$ limit line are not in a flux-limited catalog that has this apparent magnitude limit. Therefore, the mean value of H_0 is biased in this region.

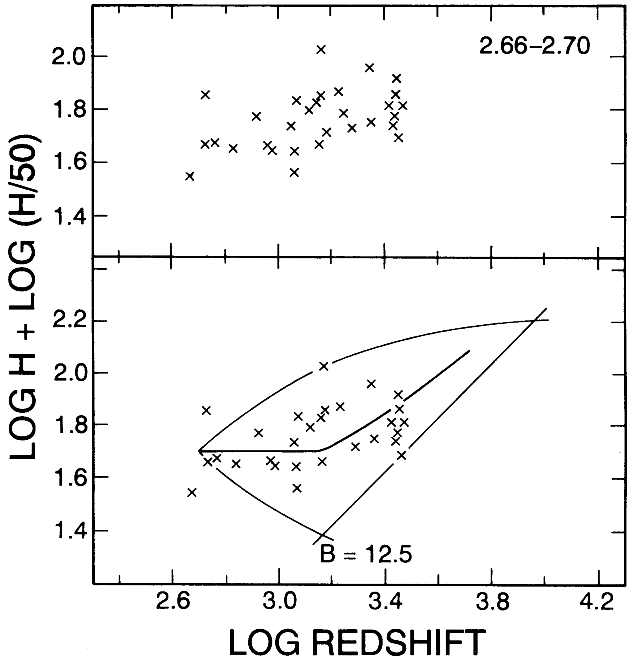

FIG. 15.—Same as Fig. 14, but for the log LW interval of 2.66–2.70. Note the smaller slope than that in Fig. 14.

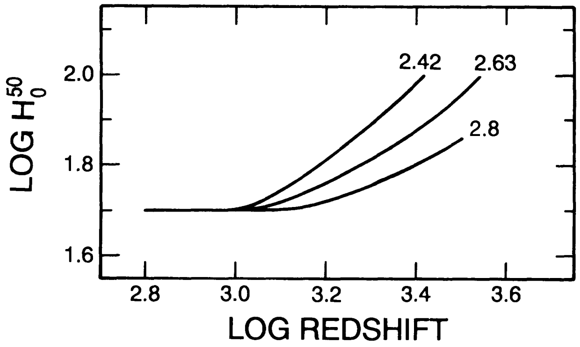

FIG. 16.—Apparent Hubble constant for the three LW intervals whose central values are marked, using the uncorrected Aaronson et al. sample in the manner of Figs. 14 and 15. Agreement of this diagram with the predictions of the *model* in Fig. 8 is excellent.

8 shows excellent agreement. The multivalued apparent Hubble constants constitute the contradiction that is the signal that selection bias exists in the sample. This is the general test for the presence of bias that can be used in any sample and with any avowed method of distance determination.

5. COMPARISON OF DISTANCE SCALES

An equivalent way of showing the bias is to compare distance scales directly in distance-distance diagrams, with and without the bias corrections of Tables 3 and 4.

Figure 17 shows the photometric distances for galaxies in the Aaronson et al. sample in the log LW interval of 2.66–2.70. The abscissa shows distances using absolute blue magnitudes that have been fully corrected via Table 3. The ordinate gives similarly corrected H-band distances using the corrections in Table 4 for the same galaxies. The zero points for the relative scales are arbitrary, based, as before, on an assumed Hubble constant of $H_0 = 50$ km s^{-1} Mpc^{-1}.

The very small scatter in Figure 17 shows that distances determined from blue magnitudes are as accurate as those determined from H magnitudes, belying the criticism that B-magnitude distances are unreliable owing to putative severe internal absorption problems. Indeed, one of the chief advantages of the blue TF relation (Fig. 11*a*) is its considerably shallower slope than the relations in photometric bandpasses further to the red. Hence, an error in the inclination correction is much less important, a point often made by others (cf. Bottinelli, Gouguenheim, & de Vaucouleurs 1983) but also often refuted (we believe incorrectly) in much of the literature on TF distances.

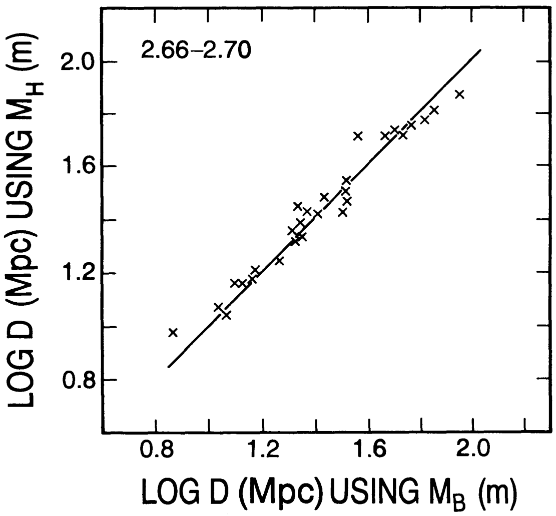

FIG. 17.—Comparison of B-band and H-band photometric distances for galaxies in the Aaronson et al. sample in the log LW interval from 2.66 to 2.70. The fully corrected B-band distances are determined using the correction curves in Fig. 13. Fully corrected photometric H-band distances are determined using a similar family of correction curves from Table 4 for H-band magnitudes.

Figure 18 (*top*) shows the fully corrected blue distances (*abscissa*) using the Table 3 (Fig. 13) corrections compared with uncorrected distances calculated by using the fixed absolute magnitude, M_0, defined by the ridge-line curve in Figure 11*a* (which is, of course, the usual, incorrect, way of applying the TF method) for the same galaxies as in Figure 17. The biased scale of the ordinate becomes progressively shorter with increasing true distance. The deviation starts at about 25 Mpc (on the scale where $H_0 = 50$), i.e., just beyond the Virgo Cluster at a distance modulus of $m - M = 31.7$.

The corrected B distance scale is compared in Figure 18 with the distances determined by Aaronson et al. in column (10) of their Table 3, relative to the distance of the Virgo Cluster. To

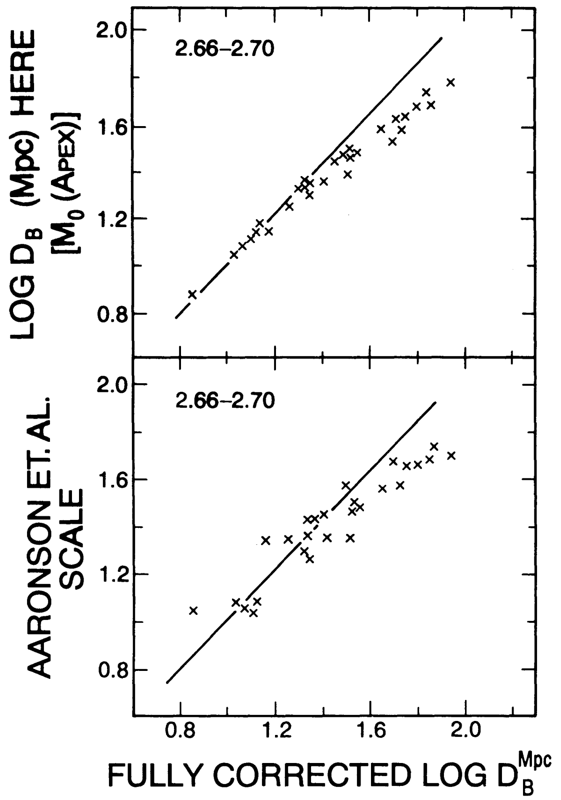

FIG. 18.—*Top*: *Fully corrected* B-band distance scale (*abscissa*) for the Aaronson et al. sample in the log LW interval of 2.66–2.70 compared with the distance scale (*ordinate*) that would have been obtained by using a fixed M_0 apex absolute magnitude of -21.2 (from Fig. 11*a*) for this LW inteval at all redshifts, i.e., with no bias corrections. The units are log distance in Mpc, based on $H_0 = 50$. Beyond 15 Mpc the distance scale along the ordinate becomes progressively, and incorrectly, compressed due to selection bias. *Bottom*: The abscissa is the same as in the top panel. The ordinate shows the uncorrected distances listed by Aaronson et al. (their Table 3) based on a Virgo Cluster distance of 22 Mpc. The systematic compression of their distance scale due to selection bias leads to an incorrectly large Hubble constant.

compare their distances with our arbitrary scale, we adopt the distance to Virgo to be 22 Mpc (Sandage & Tammann 1990), consistent with our input value of $H_0 = 50$. The resulting "absolute Aaronson" distances are plotted as ordinate. The compressed Aaronson et al. scale gives too large a value of H_0 because the biased distances are too small.

6. THE ABSOLUTE VALUE OF THE HUBBLE CONSTANT

The encomiums abroad that the Tully-Fisher method gives the strongest evidence for the short distance scale (Jacoby et al. 1992; van den Bergh 1992) are incorrect. Various TF data can be made to argue either the long or the short distance scale, depending on the sample and on the precepts. We show in this section how extant TF data require the long scale with $H_0 \sim 50$ (eqs. [3] and [6]).

Only six directly calibrated galaxies exist with adequate line-width data and Cepheid distances in the *B* photometric band, as set out in Table 5. The data are updated from those used by Sandage & Tammann (1976) and those listed in S88b (Table 3). The data here are based on the new Cepheid distance of $m - M = 27.7$ for M81 (Freedman & Madore 1988; Freedman et al. 1994, verifying the value used in Sandage & Tammann 1981 but showing that the speculation by Sandage 1984 is incorrect), and $m - M = 26.66$ for NGC 300 (Freedman et al. 1992).

Five calibrating galaxies exist in the *H* band (Freedman 1990, Table 1). The number is too small to control systematic errors in a zero-point calibration to ± 0.2 mag, required to know H_0 to within 10%. The standard deviation of the five (or six) calibrators about the TF ridge line is small at $\sigma(M_H) = 0.15$ mag in *H* (Freedman 1990) and 0.22 mag in *B* (Sandage & Tammann 1976 and Table 5 here), whereas the true dispersion of large TF samples is at least $\sigma = 0.7$ mag in *B* (§ 2.2), $\sigma = 0.6$ mag in *H*, and $\sigma = 0.6$ mag in *I*, determined here and in Paper III.

6.1. *The Absolute Calibration in B*

The six calibrators used in S88b are listed in Table 5, updated as described in the preceding paragraphs.

A calibration that is much stronger in principle was made by Richter & Huchtmeier (1984, hereafter RH84), based on 64 galaxies in seven nearby groups whose distances are presumed known by classical means. The aggregates are the Local Group and the groups associated with M81/NGC 2403, M101, the CVn I group (containing NGC 4395 and IC 4182), the Cen A group, the Sculptor group, and the CVn II group.

TABLE 5A

CALIBRATION FOR THE TF RELATION IN THE *B* PHOTOMETRIC BAND

Galaxy	$(m - M)_0$	LW	log LW	$M_{B(T)}$
M31	24.12	548	2.739	−21.41
NGC 300	26.66	221	2.344	−18.35
M33	24.7	236	2.373	−19.01
M81	27.7	498	2.697	−20.69
M101	29.2	580	2.763	−21.31

TABLE 5B

FREEDMAN'S TF CALIBRATION FOR *H*-BAND MAGNITUDES

Galaxy	$(m - M)_0$	log LW	M_H
M31	24.4	2.737	−23.49
NGC 300	26.66	2.371	−19.66
M33	24.5	2.403	−20.12
NGC 2403	27.5	2.486	−21.05
M81	27.6	2.724	−23.22

The samples are very nearly complete, based on exhaustive surveys for the group contents in the well-known classical literature (e.g., Holmberg 1950; de Vaucouleurs 1975; Kraan-Korteweg & Tammann 1979, hereafter KKT). The group distances were based on Table 2 of the first edition of the RSA (Sandage & Tammann 1981, hereafter RSA1), most of which are derived from Cepheid distances. RH84 adopted the $m - M$ distance moduli as 27.76 for the M81/NGC 2403 group, 28.76 for CVn I, for M101, and 27.76 for Sculptor. Their final $m - M$ absolute distance moduli, derived by reading their final calibrated TF relation back through itself, are 27.6 for M81/NGC 2403, 28.2 for CVn I, 29,1 for M101, and 27.2 for Sculptor. The agreement of these numbers is excellent with the current Cepheid distance moduli of $m - M = 27.6$ for M81/NGC 2403 (Tammann & Sandage 1968; Freedman & Madore 1988), 29.4 for M101 (Cook, Aaronson, & Illingworth 1986), 28.4 for IC 4182 in CVn I (Sandage et al. 1992), and 26.66 for NGC 300 in the Sculptor group (Freedman et al. 1992, but note also that NGC 300 is the closest in the Sculptor group as set out in Table 2 of RSA1).

The conclusion is that the scale adopted by RH84 is within 0.1 mag of the current local Cepheid distance scale. Therefore, their calibration is very much stronger than that based on Table 5 alone for *B* magnitudes or on Table 1 of Freedman (1990) for *H* magnitudes.

The second most satisfactory feature of the RH84 calibration is that the intrinsic dispersion of the calibrators about the mean line is 0.74 mag, close to what we expect from the external relative data as described earlier.

The absolute calibration in *B* adopted by RH84 is

$$M_{BT}^{0,i} = (-7.1 \pm 0.2) \log \mathrm{LW}_{20} - 2.12 \pm 0.10 , \qquad (1)$$

where the LW is read at the 20% level and where the *B* magnitudes are corrected for Galactic and internal absorption by the precepts of RSA1, column (15).

Comparison of equation (1) with Table 5 shows that the six calibrators define a zero point that is 0.32 mag *fainter than equation (1)*, suggesting their unfairness as a sample. With so few galaxies in the presence of the high intrinsic dispersion of $\sigma(M) = 0.74$ mag, a deviation of 0.32 mag in the average value, using only five objects, would only be a 1 σ deviation from the "true" calibration.

6.2. *The Absolute Hubble Constant Using Various Calibrations*

6.2.1. H_0 *Using the Distance-limited KKT* 500 km s^{-1} *Local Sample*

Clearly, equation (1) is the best available calibration of the TF ridge line based on a distance-limited, unbiased sample, based as it is on so much fundamental data, mostly calibrated by Cepheids. The best sample with which to use this calibration is the distance-limited 500 km s^{-1} catalog of nearby galaxies by KKT. No corrections of any kind are needed for observational selection bias because both the catalog and the calibration are based on distance-limited samples.

Huchtmeier & Richter (1986, hereafter HR86) have obtained radio line-width data for most of the KKT sample. The 21 cm line widths were reduced to edge-on orientation using the inclinations listed by HR86. The data are listed in detail elsewhere (S88b, Table 2), with fully corrected redshifts and M_B absolute magnitudes calculated from the redshift distances for the 26 suitable galaxies in the KKT sample. The distance scale used to calculate M_B magnitudes is, again, arbitrarily based on $H_0 = 50$.

The KKT field galaxy data are plotted in Figure 19 together with the six calibrating galaxies from Table 5. The least-squares ridge line for the distance-limited 26 field galaxy sample has the equation

$$M_{B_T}^{0,i} = -7.416 \log \mathrm{LW}_{20} - 1.239 \pm 0.15 , \qquad (2)$$

which is equation (7) of S88b. The dispersion about this line of $\sigma(M) = 0.74$ mag is identical to $\sigma(M)$ for the calibrating galaxies, and is close to what we have obtained from Figure 1 and what will be obtained in Paper III for the Mathewson et al. (1992) sample.

Applying equation (1) for the absolute calibration to equation (2), which is based on the arbitrary kinematic distance scale of $H_0 = 50$, gives a correction to this arbitrary scale of 0.09 mag, the calibration (eq. [1]) being brighter. Hence, applying a 0.09 mag correction to equation (2) in order to put the $M_{B_T}^{0,i}$ values on the RH84 calibration gives

$$H_0 = 48 \pm 5 \ \mathrm{km\ s^{-1}\ Mpc^{-1}} . \qquad (3)$$

The error is calculated as if the zero points in equations (1) and (2) are uncertain by 0.15 and 0.1 mag, respectively.

Had we used the calibration from Table 5 rather than the 64 galaxy calibration of RH84 (eq. [1]), we would obtain

$$H_0 = 56 \pm 5 \ \mathrm{km\ s^{-1}\ Mpc^{-1}} , \qquad (4)$$

which is higher than equation (3) because the six individual galaxies average 0.32 mag fainter than the calibration of equation (1).

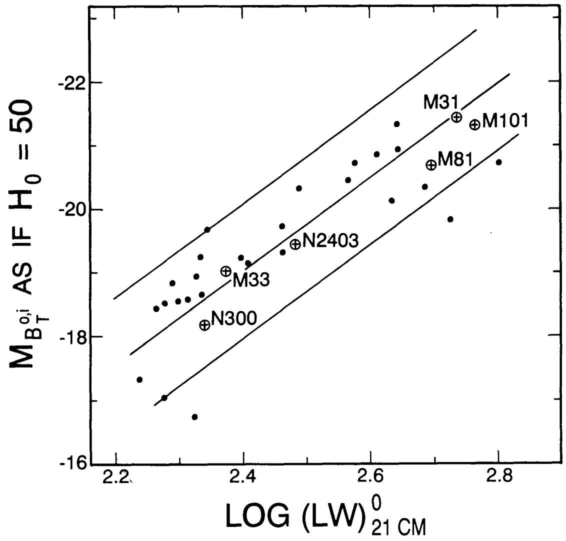

FIG. 19.—Tully-Fisher relation using fully corrected redshifts and line widths for the 26 suitable galaxies in the KKT 500 km $\mathrm{s^{-1}}$ distance-limited sample. The 21 cm line-width data are from Huchtmeier & Richter (1986). The ridge line is eq. (2) of the text. The envelope lines are placed at $\pm 1.5\ \sigma = 1.05$ mag from the ridge line. The six local calibrators from Table 5 are indicated. The zero point of the ordinate is based on an arbitrary Hubble constant of $H_0 = 50$ and a noiseless linear redshift-distance relation for the 26 sample galaxies. Any difference between the calibrators and the field galaxies signals either (1) a difference between $H_0 = 50$ and the actual H_0 value or (2) a systematic error in the mean $\langle M \rangle$ value of the calibrators due to the small sample. $H_0 \sim 85$ is not supported by these data.

6.2.2. H_0 *from the B-Band Aaronson Sample*

The equation of the ridge line in Figure 1 is

$$M_{B_T}^{0,i} = -6.77 \log \mathrm{LW}_{20} - 3.74 , \qquad (5)$$

as given by equation (3) in S88b, again on the zero point based on redshift distances with $H_0 = 50$.

The Hubble constant found by comparing equation (5) with the RH84 calibration of equation (1) is not straightforward because the Aaronson et al. sample that gives equation (5) *is fully Malmquist-biased.*

Comparing equation (1) with equation (5) over the log LW range from 2.2 to 2.8 shows an absolute magnitude offset of 0.78 mag, equation (5) being brighter. If (*a*) the dispersion is $\sigma(M) = 0.74$, given by the RH84 calibrating sample and by the other TF data we discussed earlier and will discuss in Paper III, and (*b*) the sample from Figure 1 is ideally *complete* to a given flux limit (known not to be precisely true), then applying the classical Malmquist correction of $M_0 - M(m) = 1.386\ \sigma(M)^2 = 0.76$ mag would leave the Figure 1 data, corrected for bias, too bright by 0.02 mag relative to the arbitrary distance scale based on $H_0 = 50$. The result, corrected in this way for bias using $\sigma(M) = 0.74$ mag, is then

$$H_0 = 51 \ \mathrm{km\ s^{-1}\ Mpc^{-1}} . \qquad (6)$$

On the other hand, if the true dispersion is $\sigma(M) = 0.64$ mag as in Figure 1, then the bias correction is reduced to 0.57 mag (S88b), giving

$$H_0 = 55 \ \mathrm{km\ s^{-1}\ Mpc^{-1}} , \qquad (7)$$

again using the absolute calibration of RH84 (eq. [1]).

A second method is to use that portion of the total Aaronson et al. sample in *B that is unbiased.* This is the subsample that defines the M_0 ridge line in Figure 11*a* using the *apex* magnitudes of the individual Spaenhauer diagrams for the various line widths. The equation of the ridge line using data in Table 2 is

$$M_{B_T}^{0,i} = -6.86 \log \mathrm{LW}_{20} - 3.02 . \qquad (8)$$

Applying the RH84 calibration of equation (1) to equation (8) over the relevant log LW range gives a correction of 0.29 mag, the RH84 calibration being fainter, giving

$$H_0 = 57 \pm 5 \ \mathrm{km\ s^{-1}\ Mpc^{-1}} . \qquad (9)$$

Finally, we could use only the six *B*-band calibrators in Table 5 with equation (8) for the unbiased part of the Aaronson et al. sample. Because these calibrators average 0.32 mag fainter than the RH84 calibration in equation (1), equation (9) becomes

$$H_0 = 66 \ \mathrm{km\ s^{-1}\ Mpc^{-1}} . \qquad (10)$$

This is the least probable of the calibrations because, as we have argued, the six calibrators are probably too faint.

Note that all of the blue-band data with the highest weight give Hubble constants (eqs. [3], [6], [7], and [9]) that support the long distance scale. This fact was not emphasized in the summaries of Jacoby et al. (1992) and van den Bergh (1992). But what they do set out is the contrary conclusion based on the *H*-band data, which we now discuss.

6.2.3. H_0 *from the H-Band Aaronson Sample*

Freedman (1990) lists the five fundamental calibrators in *H*. These can be used in two ways with the Aaronson *H*-band data.

1. The ridge line in Figure 11*b* for the *distance-limited* subsample using the apex absolute magnitudes has the equation

$$M_H^0(H = 50) = -10.56 \log \mathrm{LW}_{20} + 4.37 , \qquad (11)$$

based on redshift distances with the arbitrary value of $H_0 = 50$. This equation predicts M_H magnitudes for the five fundamental standards that average 0.99 mag brighter than the values listed by Freedman, requiring a change in the calculated zero point of the adopted redshift distances by a factor of antidex $(0.99/5) = 1.58$, giving a Hubble constant of $H_0 = 79$ km s^{-1} Mpc^{-1} (see also S88b). However, if the mean of this calibrator is too faint by 0.32 mag as we suspect for the *B* band, this value would be reduced to

$$H_0 = 68 \text{ km s}^{-1} \text{ Mpc}^{-1} . \qquad (12)$$

2. The ridge line for the total Aaronson sample (Fig. 11*b*, *dashed line*) has the equation

$$M_H = -10.84 \log \mathrm{LW}_{20} + 4.82 , \qquad (13)$$

from equation (2) of S88b, again on a distance scale with $H_0 = 50$. The five calibrators of Freedman average 1.25 mag fainter than is predicted for them using equation (13). This is reduced to 0.93 mag if again the calibrators are 0.32 mag too faint.

However, this sample carries the total Malmquist bias because it is not distance-limited. If $\sigma(M_H) = 0.56$ as calculated in S88b for the Aaronson *H*-band sample, then the Malmquist ensemble correction is 0.43 mag. Hence, the distance-scale correction is $0.93 - 0.43 = 0.50$ mag via this route, or

$$H_0 = 63 \text{ km s}^{-1} \text{ Mpc}^{-1} . \qquad (14)$$

In summary, all *B*-band distances support the long scale ($H_0 < 60$). All *H*-band distances require $H_0 < 80$, or, after zero-point correction of the calibrators, $H_0 < 70$. Hence, the TF relation using field galaxies does not in any of the cases support the short distance scale ($H_0 > 80$), whereas all of the *B*-band TF data require the long scale with $H_0 \sim 50$ km s^{-1} Mpc^{-1} (Fig. 19).

7. DISCUSSION AND CONCLUSIONS

Arguments in criticism of Paper I, of the present paper, and of Paper III will be of two types:

A. The method of correcting for bias via the Spaenhauer diagrams will be argued to be circular—the derived corrections to absolute magnitudes being nothing more than what is required to maintain an *assumed* linearity that itself has been put in the model ab initio.

B. The methods to obtain H_0 in § 6 will be argued to be unreliable because they are based on field galaxy samples rather than "cluster" and "group" samples which show putative much smaller dispersions for the derived Tully-Fisher correlation. Because of this, it will also be claimed that the corrections set out in Tables 3 and 4 are gross overestimates because large enough peculiar motions exist to cause the redshift distances to have large individual errors, spuriously producing the large dispersions of $\sigma(M) > 0.6$ derived here and previously (S88b).

7.1. *Circularity?*

Have we committed circular reasoning by requiring a noiseless linear redshift-distance relation and then calculating the photometric bias corrections (Table 1 of Paper I and Tables 3 and 4 of this paper) to make it so? The problem is discussed in different terms in § 2 of Paper I and in § 7.2, footnote 4, and § 8 of Paper III. It is shown in both places that the criticism is incorrect.

1. From many experiments cited previously it is known that the global redshift-distance relation is linear to as high an accuracy as we can measure it. This is better than $\pm 2\%$ (globally) for the exponent $n = 1$ in $v \sim r^n$ (Sandage, Tammann, & Hardy 1972; Lauer & Postman 1992; Jerjen & Tammann 1993). It is, of course, true that a streaming motion has been discovered via the 600 km s^{-1} dipole of the cosmic microwave background, showing a relatively local ($v < 4000$ km s^{-1}) perturbation of an ideal Hubble flow, but only in a particular direction of the sky, defining the kinematics of the "local region" related to the direction of the CMB (see Paper III for the model).

2. The systematic cosmological expansion begins just beyond the local Group, and has a random velocity component that has $\sigma < 50$ km s^{-1} Mpc^{-1} about the Hubble flow locally (Sandage 1986, Figs, 7, 9, and 10; Sandage 1987, Figs. 1, 5, and 6).

3. The large dispersion in absolute magnitude (at a given line width) obtained when using redshift distances is not an artifact of incorrect cosmological redshifts that would be induced by large pecular motions. As discussed in § 2.2, the signature in a Spaenhauer diagram of any real velocity anomalies due to peculiar motions would be a high dispersion in the derived absolute magnitude *at low redshift*, becoming *smaller* at high redshifts; i.e., $\Delta v/v_c$ becomes smaller. This is the opposite of what is observed. The envelope lines that enclose the data in the Spaenhauer configurations of Figures 9 and 10 in § 3 open *outward* with increasing redshift.

4. The model accounting for selection bias derived in this series gives predictions concerning the nature of the absolute magnitude corrections at each redshift, at each line width, and at each arbitrary cut in the apparent magnitude limit of a flux-limited catalog. These predictions are consistent with the observations in every detail (Figs. 4, 7, 8, 14, 15, and 16, and Fig. 5 compared with Fig. 13), giving a picture with no contradictions. Furthermore, the same model also explains the systematics in the TF relations at each line width and redshift of the very large TF sample of Mathewson et al. (1992) discussed in Paper III. It is (*a*) the consistency of the models, (*b*) their predictive power concerning the observations, fully verified, (*c*) the detailed systematics of the variation of the biased apparent Hubble constant changes with redshift and with line width (e.g., Figs. 2 and 3 of Paper III), and (*d*) the knowledge from external sources that the redshift-distance relation *is* linear that ensures the noncircularity of the argument here.

7.2. *Status of the Tully-Fisher Method for Determining H_0 and Deviations from a Noiseless Hubble Flow*

The purpose of § 6 is not only to obtain a reliable value of H_0 per se but also to demonstrate that values of the Hubble constant via the TF method can be derived that support either the long or the short distance scale, depending on the adopted precepts. It is, therefore, incorrect to state that the Tully-Fisher method provides decisive proof for the short scale with $H_0 \sim 85$ (Jacoby et al. 1992; van den Bergh 1992).

It has been emphasized that the bias corrections, derived from these methods, vary with the limiting magnitude of each catalog. They must, therefore, be determined anew for each catalog from its internal properties. Failure to do so will produce systematically incorrect photometric distances that will cause false conclusions concerning the nature of the velocity field within the range of the catalog. One of the consequences is an apparent, but incorrect, increase of the Hubble constant outward. Potentially even more serious are the claims for large streaming motions superposed on the cosmological expansion field, found by comparing derived photometric distances with redshift distances and interpreting the differences as real.

It is our thesis that the bias properties of each sample must be investigated by methods that use data inherent in the Spaenhauer diagrams themselves. Until then, claims of streaming motions will remain unproved until it is shown that the photometric distances have greater systematic accuracies than redshift distances and therefore that the differences between them are real. A further discussion of streaming motions, real and artificial, is given in Paper III (§ 8).

The first drafts of this paper were written while the author was a visitor at the Institute of Astronomy of the University of Basel. I am grateful for the hospitality of G. A. Tammann and the staff of the Institute during an extended stay. It is also a pleasure to acknowledge discussions with Tammann on this and similar problems over the past two decades. He also read a later draft of the paper while he was in Pasadena, and he made important suggestions concerning it as a prelude to Paper III that follows.

REFERENCES

Aaronson, M., Huchra, J., Mould, J., Schechter, P., & Tully, R. B. 1982a, ApJ, 258, 64
Aaronson, M., et al. 1982b, ApJS, 50, 241
Bottinelli, L., Gouguenheim, L., & de Vaucouleurs, G. 1983, A&A, 118, 4
Bottinelli, L., Gouguenheim, L., Paturel, G. R., & Teerikorpi, P. 1986, A&A, 156, 157
Cook, K., Aaronson, M., & Illingworth, G. 1986, ApJ, 301, L45
de Vaucouleurs, G. 1975, in Stars and Stellar Systems, Vol. 9, Galaxies and the Universe, ed. A. Sandage, M. Sandage, & J. Kristian (Chicago: Univ. Chicago Press), 14
de Vaucouleurs, G., & Peters, W. L. 1986, ApJ, 303, 19
Dressler, A., & Faber, S. M. 1990a, ApJ, 354, 13
———. 1990b, ApJS, 354, L45
Federspiel, M., Sandage, A., & Tammann, G. A. 1994, ApJ, 430, 29 (Paper III)
Freedman, W. L. 1990, ApJ, 355, L35
Freedman, W. L., & Madore, B. F. 1988, ApJ, 332, L63
Freedman, W. L., et al. 1994, ApJ, in press
Freedman, W. L., Madore, B. F., Hawley, S. L., Horowitz, I. K., Mould, J., & Navarrete, M. 1992, ApJ, 396, 80
Giraud, E. 1985, A&A, 153, 125
———. 1986a, ApJ, 301, 7
———. 1986b, ApJ, 309, 312
———. 1986c, A&A, 174, 23
Holmberg, E. 1950, Medd. Lunds Astron, Obs., Ser. 2, No. 128
Huchtmeier, W. K., & Richter, O.-G. 1986, A&AS, 63, 325 (HR86)
Jacoby, G., et al. 1992, PASP, 104, 599
Jerjen, H., & Tammann, G. A. 1993, A&A, 276, 1
Kraan-Korteweg, R. C. 1986a, A&AS, 26, 509
———. 1986b, A Catalog of 2810 Nearby Galaxies (Basel Publ. Ser., No. 18)
Kraan-Korteweg, R. C., Cameron, L. M., & Tammann, G. A. 1986, in Galaxy Distances and Deviations from Universal Expansion, ed. B. F. Madore & R. B. Tully (Dordrecht: Reidel), 65
Kraan-Korteweg, R. C., Cameron, L. M., & Tammann, G. A. 1988, ApJ, 331, 620
Kraan-Korteweg, R. C., & Tammann, G. A. 1979, Astron. Nach., 300, 181
Lauer, R. R., & Postman, M. 1992, ApJ, 400, L47
Malmquist, G. 1920, Lund Medd., Ser., No. 22
Mathewson, D. S., Ford, V. L., & Buchhorn, M. 1992, ApJS, 81, 413
Pierce, M., & Tully, R. B. 1992, ApJ, 387, 47
Richter, O.-G., & Huchtmeier, W. K. 1984, A&A, 132, 253 (RH84)
Sandage, A. 1984, AJ, 89, 621
———. 1986, ApJ, 307, 1
———. 1987, ApJ, 317, 557
———. 1988a, ApJ, 331, 583 (S88a)
———. 1988b, ApJ, 331, 605 (S88b)
———. 1994, ApJ, 430, 1 (Paper I)
Sandage, A., Saha, A., Tammann, G. A., Panagia, N., & Macchetto, D. 1992, ApJ, 401, L7
Sandage, A., & Tammann, G. A. 1976, ApJ, 210, 7
———. 1981, 1987, A Revised Shapley-Ames Catalog of Bright Galaxies (Carnegie Inst. Washington Publ. 635) (RSA1, RSA2)
———. 1990, ApJ, 365, 1
Sandage, A., Tammann, G. A., & Hardy, E. 1972, ApJ, 172, 253
Schechter, P. 1980, AJ, 85, 801
Tammann, G. A., & Sandage, A. 1968, ApJ, 151, 825
———. 1985, ApJ, 294, 81
Teerikorpi, P. 1984, A&A, 141, 407
———. 1987, A&A, 173, 39
———. 1990, A&A, 234, 1
Tully, B. 1988, Nature, 334, 209
van den Bergh, S. 1992, PASP, 104, 861